

Article

ZnO Nanocrystal-Based Chloroform Detection: Density Functional Theory (DFT) Study

H. Y. Ammar^{1,2,3,*}, H. M. Badran^{1,2,3}, Ahmad Umar^{1,4,*}, H. Fouad^{5,6,*} and Othman Y. Alothman⁷

- ¹ Promising Centre for Sensors and Electronic Devices (PCSED), Najran University, Najran 11001, Saudi Arabia; drhebadran@gmail.com
- ² Department of Physics, Faculty of Science and Arts, Najran University, Najran 11001, Saudi Arabia
- ³ Physics Department, Faculty of Education, Ain Shams University, Cairo 11566, Egypt
- ⁴ Department of Chemistry, Faculty of Science and Arts, Najran University, Najran 11001, Saudi Arabia
- ⁵ Department of Applied Medical Science, Community College, King Saud University, Riyadh 11437, Saudi Arabia
- ⁶ Biomedical Engineering Department, Faculty of Engineering, Helwan University, P.O. Box, Helwan 11792, Egypt
- ⁷ Chemical Engineering Department, King Saud University, P. O. Box 800, Riyadh 11421, Saudi Arabia; othman@ksu.edu.sa
- * Correspondence: hyammar@hotmail.com (H.Y.A.); umahmad@nu.edu.sa or ahmadumar786@gmail.com (A.U.); menhfef@ksu.edu.sa (H.F.)

Received: 5 October 2019; Accepted: 14 November 2019; Published: 19 November 2019



Abstract: We investigated the detection of chloroform (CHCl₃) using ZnO nanoclusters via density functional theory calculations. The effects of various concentrations of CHCl₃, as well as the deposition of O atoms, on the adsorption over ZnO nanoclusters were analyzed via geometric optimizations. The calculated difference between the highest occupied molecular orbital and the lowest unoccupied molecular orbital for ZnO was 4.02 eV. The most stable adsorption characteristics were investigated with respect to the adsorption energy, frontier orbitals, elemental positions, and charge transfer. The results revealed that ZnO nanoclusters with a specific geometry and composition are promising candidates for chloroform-sensing applications.

Keywords: nanocrystal; ZnO; density of states; optical and electrical properties

1. Introduction

The rapid development of various important industries, such as automobiles, pharmaceuticals, textiles, food, and agriculture, has substantially contributed to environmental pollution [1]. The release of various toxic and harmful gases and chemicals from such industries has significantly disturbed the ecosystem, and poses a great threat not only to humans, but to all living beings [2,3]. Among the various toxic gases, chloroform, which is also known as tri-chloromethane or methyl-tri-chloride, is considered to be one of the most toxic gases, and evaporates quickly when exposed to air [4]. It is widely used by chemical companies and in paper mills. Chloroform lasts for a long time in the environment, and its breakdown products, such as phosgene and hydrogen chloride, are as toxic or even more toxic [5]. The exposure of humans to chloroform severely affects the central nervous system, kidneys, liver, etc. Long-term exposure may result in vomiting, nausea, dizziness, convulsions, depression, respiratory failure, coma, and even sudden death [6,7]. It is important to efficiently detect the release of chloroform because of its serious health hazards. Thus, various methods have been reported for detecting chloroform, which involve optical sensors, colorimetric sensors, fluorescent

sensors, electrochemical sensors, resistive gas sensors, luminescent sensors, photo-responsive sensors, etc. [8–13].

Among the various sensing techniques, gas sensors have attracted considerable attention because of their facile manufacturing process, high sensitivity, and low detection limit [14–17]. The literature reveals that metal-oxide materials are the most widely used scaffold to fabricate gas sensors [15–20]. In particular, metal-oxide materials are widely utilized to fabricate sensors for toxic and explosive gases [20–24]. It has been observed that the nanocrystal interfaces can significantly influence the optical and electrical properties and charge-trapping phenomena [22–25]. Zinc oxide (ZnO) is one of the most important and functional materials because of its various significant properties, including its wide bandgap; high exciton binding energy, piezoelectricity, and pyroelectricity; high conductivity and electron mobility; good stability in chemical and thermal environments; and biocompatibility [26–28]. Therefore, to improve the gas-sensing performance of ZnO-based gas sensors, various approaches have been employed, such as doping, surface modification, and the fabrication of composites [26,29]. Although ZnO materials are used for various gas-sensing applications [30–34], there are few reports available on the use of ZnO materials for chloroform sensing. Ghenaatian et al. [35] investigated the $Zn_{12}O_{12}$ nanocage as a promising adsorbent and detector for CS_2 . Baie et al. examined the $Zn_{12}O_{12}$ fullerene-like cage as a potential sensor for SO_2 detection [36]. Ammar [37] reported that the $Zn_{12}O_{12}$ nanocage is a potential sorbent and detector for formaldehyde molecules. Nanocrystalline ZnO thin-film gas sensors were investigated by Mayya et al. [38] for the detection of hydrochloric acid, ethanolamine, and chloroform. Additionally, it is important to examine various geometries and other electronic parameters in order to obtain the optimal sensing material based on ZnO.

In this study, we investigated the detection of chloroform ($CHCl_3$) using ZnO nanoclusters via density functional theory (DFT) calculations implemented in a Gaussian 09 program. The effect of various concentrations of $CHCl_3$, as well as the deposition of O atoms, on the adsorption over ZnO nanoclusters was analyzed via geometric optimizations. To fully exploit the ZnO nanocrystals, various calculations related to the gas-sensing properties were performed.

2. Methods and Computational Details

A quantum cluster consisting of 24 atoms ($Zn_{12}O_{12}$) was selected to study the interaction between the ZnO nanocage and the $CHCl_3$ molecule. DFT calculations were performed with the Gaussian 09 suite of programs [39]. The calculations were conducted using Becke's three-parameter B3 with the Lee, Yang, and Parr (LYP) correlation functional [40]. This B3LYP hybrid functional contains the exchange–correlation functional, and is based on the exact form of the Vosko–Wilk–Nusair correlation potential [41]. Originally, the functional B included the Slater exchange along with corrections involving the gradient of density [42]. The correlation functional LYP was that of Lee, Yang, and Parr, which includes both local and nonlocal terms [43,44]. For the ZnO nanocage, the standard LANL2DZ basis set [37,45] was used. For the $CHCl_3$ and the deposited O atoms, a 6-31G (d, p) basis set was used. The adsorption energy (E_{ads}) of the $CHCl_3$ molecule on the surface of the $Zn_{12}O_{12}$ nanocage is defined as follows:

$$E_{ads} = \left[E_{(CHCl_3)_n/ZnO} - (nE_{CHCl_3} + E_{ZnO}) \right] / n, \quad (1)$$

where E_{CHCl_3} , E_{ZnO} and $E_{(CHCl_3)_n/ZnO}$ represent the energies of a single $CHCl_3$ molecule, the pristine $Zn_{12}O_{12}$ nanocage, and the $(CHCl_3)_n/Zn_{12}O_{12}$ complex, respectively.

The adsorption energy (E_{ads}) of an O atom on the surface of the $Zn_{12}O_{12}$ nanocage is defined as follows:

$$E_{ads} = \left[E_{O_n/ZnO} - (nE_O + E_{ZnO}) \right] / n, \quad (2)$$

where E_O and $E_{O_n/ZnO}$ represent the energies of a single O atom and the $O_n/Zn_{12}O_{12}$ complex, respectively.

The adsorption energy (E_i) of a CHCl_3 molecule on the deposited O on the $\text{Zn}_{12}\text{O}_{12}$ nanocage is defined as follows:

$$E_i = \left[E_{(\text{CHCl}_3)_n/\text{O}_n/\text{ZnO}} - (nE_{\text{CHCl}_3} + nE_{\text{O}} + E_{\text{ZnO}}) \right] / n, \quad (3)$$

where $E_{(\text{CHCl}_3)_n/\text{O}_n/\text{ZnO}}$ represents the energy of the $(\text{CHCl}_3)_n/\text{O}_n/\text{ZnO}$ complex.

The positive and negative values of E_i indicate the endothermic and exothermic processes, respectively. The binding energy (E_b) between the X and Y fragments of the XY complex is defined as follows:

$$E_b = E_{XY} - (E_X + E_Y), \quad (4)$$

where E_{XY} represents the total energy of the optimized molecule, and E_X and E_Y represent the energies of the two fragments X and Y, respectively, having the same geometric structure as in the XY complex. The GaussSum 2.2.5 program was used to calculate the densities of states (DOSs) for the $\text{Zn}_{12}\text{O}_{12}$ nanocage, CHCl_3 , and other complex systems [46]. Full natural bond orbital (NBO; NBO version 3.1) analyses were used to estimate the charge distributions for the $\text{Zn}_{12}\text{O}_{12}$ nanocages, CHCl_3 , and other complex systems [47].

3. Results and Discussion

3.1. Geometric Optimization

The geometric optimization of a pristine $\text{Zn}_{12}\text{O}_{12}$ nanocage was performed. $\text{Zn}_{12}\text{O}_{12}$ is composed of eight $(\text{ZnO})_3$ and six $(\text{ZnO})_2$ rings, forming a cluster in which all of the Zn and O vertices are equivalent [48], as shown in Figure 1. The examined structural properties of the $\text{Zn}_{12}\text{O}_{12}$ nanocage agreed well with previous studies [37,45,49]. For example, the bond lengths $R_{\text{Zn-O}}$ of 1.91 and 1.98 Å were close to the previously reported values of 1.91 and 1.98 Å, respectively [37,45], and 1.89 and 1.97 Å, respectively [47]. The calculated highest occupied molecular orbital (HOMO)–lowest unoccupied molecular orbital (LUMO) energy gap for ZnO was found to be 4.02 eV, which agrees well with a previous work [45].

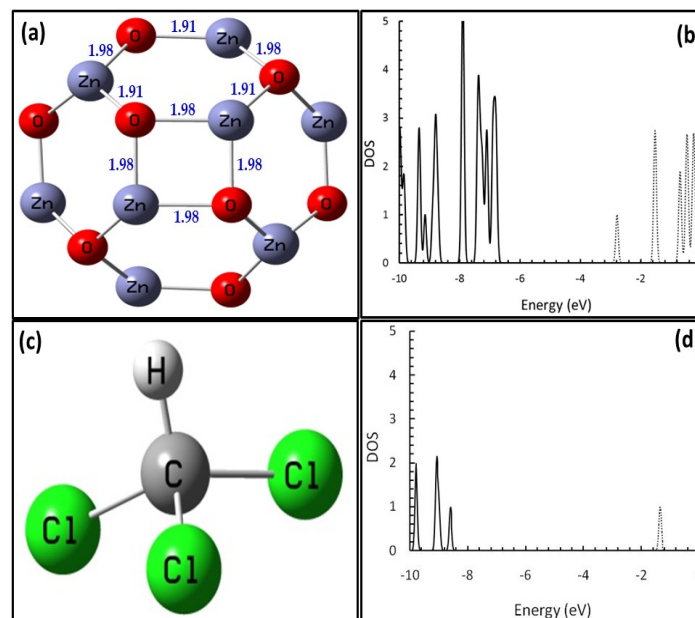


Figure 1. Optimized structures and densities of states (DOSs) of the ZnO nanocage ($\text{Zn}_{12}\text{O}_{12}$) and CHCl_3 used in the calculations. (a,b) Optimized structure and DOS of the ZnO nanocage; (c,d) optimized structure and DOS of CHCl_3 . The distances are in Å, and the DOS is in arbitrary units. The solid and dashed lines represent the occupied and virtual states, respectively.

The DOS of the $Zn_{12}O_{12}$ nanocage was calculated, as shown in Figure 1. A geometric optimization was performed for the chloroform molecule ($CHCl_3$). It is a tetrahedral molecule, as shown in Figure 1. The calculated structural properties of $CHCl_3$ indicated that bond lengths R_{C-H} and R_{C-Cl} were 1.09 and 1.79 Å, respectively, and angles A_{H-C-Cl} and $A_{Cl-C-Cl}$ were 107.5° and 11.4°, respectively. The energy gap (E_g) between the HOMO and LUMO was calculated to be 7.27 eV. The DOS for $CHCl_3$ was calculated, and is presented in Figure 1.

3.2. $CHCl_3$ Interaction with the $Zn_{12}O_{12}$ Nanocage

The geometric optimizations for four probable orientations of $CHCl_3$ on the surface of the $Zn_{12}O_{12}$ nanocage were investigated. Figure 2 shows the four orientations where the $CHCl_3$ molecule may interact via its H head or Cl head, and may be absorbed over the O site or Zn site of the $Zn_{12}O_{12}$ nanocage. The adsorption energy was calculated using Equation (1). The electronic properties of the $CHCl_3$ adsorption modes are presented in Table 1. For the first adsorption mode (a), the $CHCl_3$ molecule was weakly chemically adsorbed, and for the other modes (b, c, and d), the $CHCl_3$ molecule was physically adsorbed. The boundary value between the physical and chemical adsorption was considered to be 0.21 eV [50,51]. In mode (a), owing to the chemical interaction, the Fermi level (E_{FL}) for the cluster was reduced by 0.17 eV, and the dipole moment (D) was increased to 3.05 Debye. There was no noticeable change in the HOMO–LUMO energy gap. In all of the adsorption modes, it was found that the HOMO–LUMO energy gaps of the $CHCl_3/ZnO$ complexes were in the range of 4.00–4.03 eV. Consequently, the adsorption of $CHCl_3$ on the ZnO nanocage had no significant effect on the HOMO–LUMO energy gap.

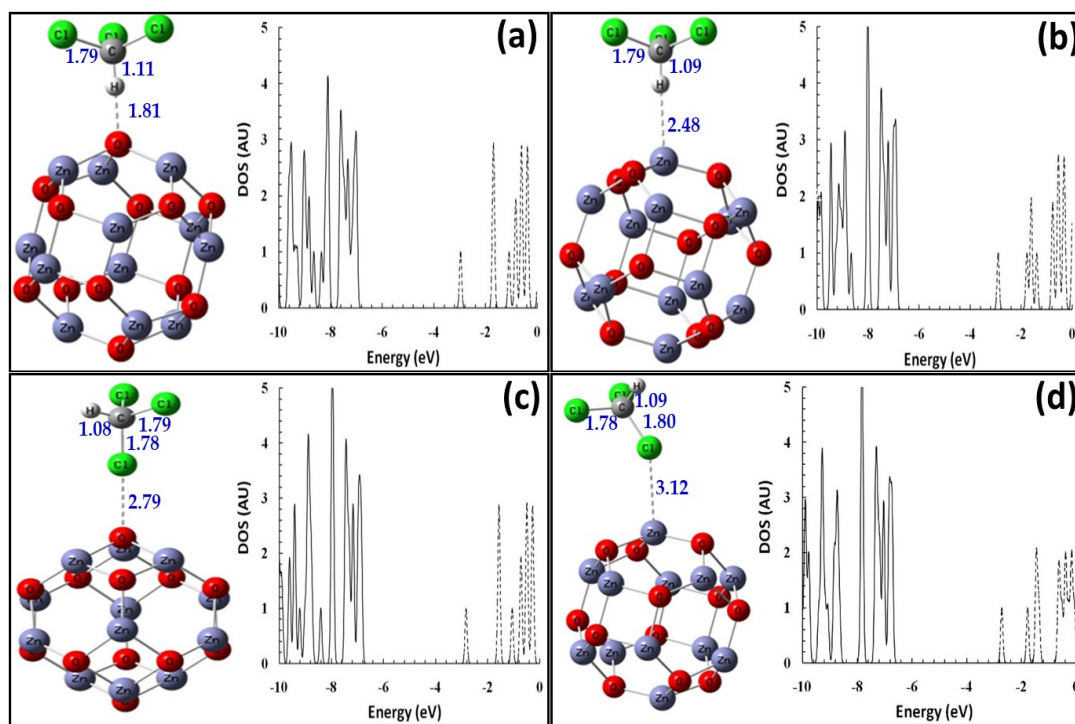


Figure 2. Optimized structures and DOSs of the $CHCl_3$ molecule adsorption on the $Zn_{12}O_{12}$ nanocage. (a) adsorption mode a, (b) adsorption mode b, (c) adsorption mode c, and (d) adsorption mode d. The distances are in Å, and the DOS is in arbitrary units. The solid and dashed lines represent occupied and virtual states, respectively.

Table 1. Electronic properties of the isomeric configurations of the $\text{CHCl}_3/\text{Zn}_{12}\text{O}_{12}$ complexes, namely: adsorption energy (E_{ads} ; eV), HOMO (eV), LUMO (eV), Fermi level (E_{FL} ; eV), HUMO–LUMO energy gap (E_g ; eV), natural bond orbital (NBO) charge (Q ; au), and dipole moment (D ; Debye).

System	Bare $\text{Zn}_{12}\text{O}_{12}$	(a)	(b)	(c)	(d)
E_{ads}	–	–0.38	0.07	–0.09	–0.04
E_{HOMO}	–6.81	–6.98	–6.90	–6.84	–6.71
E_{LUMO}	–2.79	–2.96	–2.89	–2.82	–2.71
E_{FL}	–4.80	–4.97	–4.90	–4.83	–4.71
E_g	4.02	4.03	4.00	4.02	4.00
Q_{CHCl_3}	–	–0.02	0.00	–0.01	0.02
D	0.00	3.05	1.41	1.33	2.17

Additionally, to investigate the effect of the CHCl_3 concentration on the adsorption over the $\text{Zn}_{12}\text{O}_{12}$ nanocage, we performed geometric optimizations for n CHCl_3 molecules ($n = 1, 2, 3$, and 4) adsorbed simultaneously over the $\text{Zn}_{12}\text{O}_{12}$ nanocage to form $(\text{CHCl}_3)_n/\text{ZnO}$ complexes. All of the CHCl_3 molecules had an orientation in which the H head of the CHCl_3 molecule was directed toward an O site of the $\text{Zn}_{12}\text{O}_{12}$ nanocage, which is the most energetic stable orientation, as presented in Figure 2. The adsorption energies (E_{ads}) were calculated using Equation (1), and are presented in Table 2.

Table 2. Electronic properties of the $(\text{CHCl}_3)_n/\text{Zn}_{12}\text{O}_{12}$ complexes, namely: adsorption energy (E_{ads} ; eV), HOMO (eV), LUMO (eV), Fermi level (E_{FL} ; eV), HUMO–LUMO energy gap (E_g ; eV), NBO charge (Q ; au), and dipole moment (D ; Debye).

System	(a)	(b)	(c)	(d)
	$n = 1$	$n = 2$	$n = 3$	$n = 4$
E_{ads}	–0.38	–0.38	–0.60	–0.76
E_{HOMO}	–6.98	–7.14	–7.19	–7.39
E_{LUMO}	–2.96	–3.10	–3.14	–3.32
E_{FL}	–4.97	–5.12	–5.16	–5.36
E_g	4.03	4.04	4.05	4.07
Q_{CHCl_3}	–0.02	–0.02	–0.02	–0.01
D	3.05	0.46	1.18	1.64

The optimized structures of $(\text{CHCl}_3)_n/\text{ZnO}$ and their DOSs are shown in Figure 3. As indicated by Table 2, after the second molecule was adsorbed, the adsorption energy (E_{ads}) increased as n —the number of adsorbed CHCl_3 molecules—increased. Additionally, as the number of adsorbed CHCl_3 molecules increased, the Fermi level decreased. Furthermore, although there were no significant changes in the average acquired charge (Q_{CHCl_3}) on the CHCl_3 molecules, the dipole moment was sensitive to the number of adsorbed CHCl_3 molecules. The HOMO–LUMO energy gap (E_g), compared with that of the pristine $\text{Zn}_{12}\text{O}_{12}$ nanocage (4.02 eV), was not affected by the number of adsorbed CHCl_3 molecules.

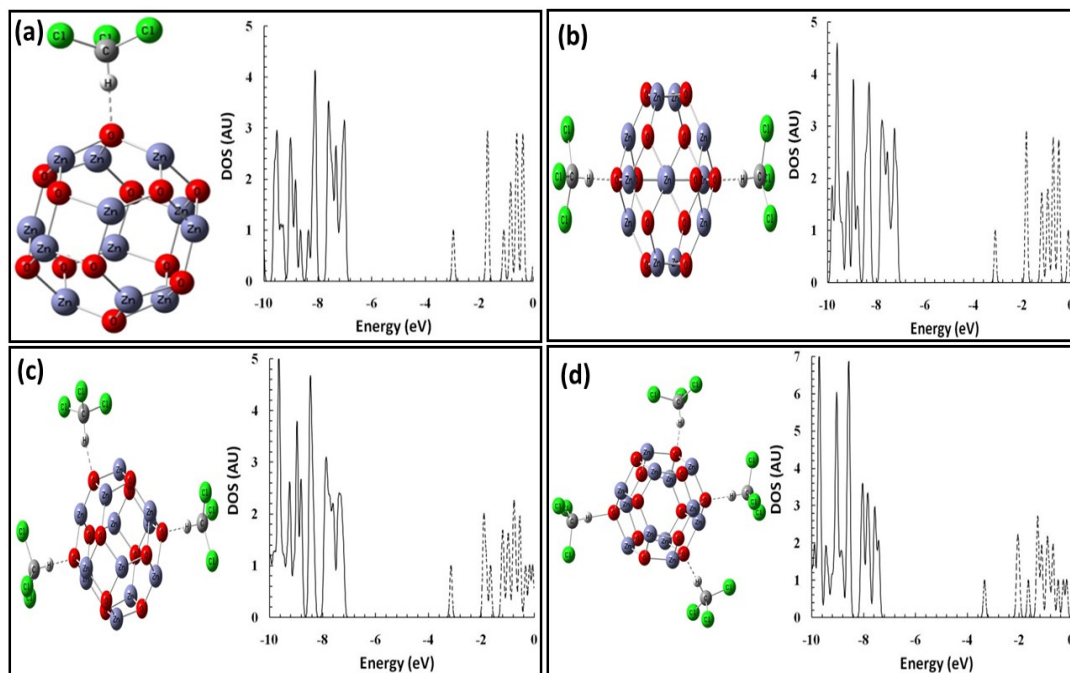


Figure 3. Optimized structures and DOSs for the $(\text{CHCl}_3)_n/\text{Zn}_{12}\text{O}_{12}$ nanocage. (a) $\text{CHCl}_3/\text{Zn}_{12}\text{O}_{12}$, (b) $(\text{CHCl}_3)_2/\text{Zn}_{12}\text{O}_{12}$, (c) $(\text{CHCl}_3)_3/\text{Zn}_{12}\text{O}_{12}$, and (d) $(\text{CHCl}_3)_4/\text{Zn}_{12}\text{O}_{12}$. The distances are in Å, and the DOS is in arbitrary units. The solid and dashed lines represent the occupied and virtual states, respectively.

3.3. O Atom Interaction with the $\text{Zn}_{12}\text{O}_{12}$ Nanocage

To improve the sensitivity of $\text{Zn}_{12}\text{O}_{12}$ to the CHCl_3 molecules, an O atom was deposited onto the cluster. To investigate the ability of the $\text{Zn}_{12}\text{O}_{12}$ nanocage to adsorb an O atom, the O atom was added at three different sites, namely: an O site, a Zn site, and the middle of the ZnO bond. Then, a full geometric optimization was performed for the $\text{O}/\text{Zn}_{12}\text{O}_{12}$ complexes. With the optimization, there are only two possible $\text{O}/\text{Zn}_{12}\text{O}_{12}$ complexes, as shown in Figure 4. The E_{ads} were calculated using Equation (2). As shown in Table 3, the E_{ads} values of the O atom on the $\text{Zn}_{12}\text{O}_{12}$ nanocage were -1.98 and -1.62 eV for complexes (a) and (b), respectively. This indicated that a chemical bond was formed between the O atom and the $\text{Zn}_{12}\text{O}_{12}$ cluster. Additionally, the NBO analysis indicated that the O atom gained negative charges (Q_{O}) of $-0.71|e|$ and $-0.61|e|$ for complexes (a) and (b), respectively.

Table 3. Electronic properties of the isomeric configurations of the $\text{O}/\text{Zn}_{12}\text{O}_{12}$ complexes, namely: adsorption energy (E_{ads} ; eV), HOMO (eV), LUMO (eV), Fermi level (E_{FL} ; eV), HUMO–LUMO energy gap (E_{g} ; eV), NBO charge (Q ; au), and dipole moment (D ; Debye).

System	$\text{O}/\text{Zn}_{12}\text{O}_{12}$	
	(a)	(b)
E_{ads}	-1.98	-1.62
E_{HOMO}	-6.32	-6.57
E_{LUMO}	-2.79	-2.79
E_{FL}	-4.56	-4.68
E_{g}	3.53	3.78
Q_{O}	-0.71	-0.61
D	2.03	0.72

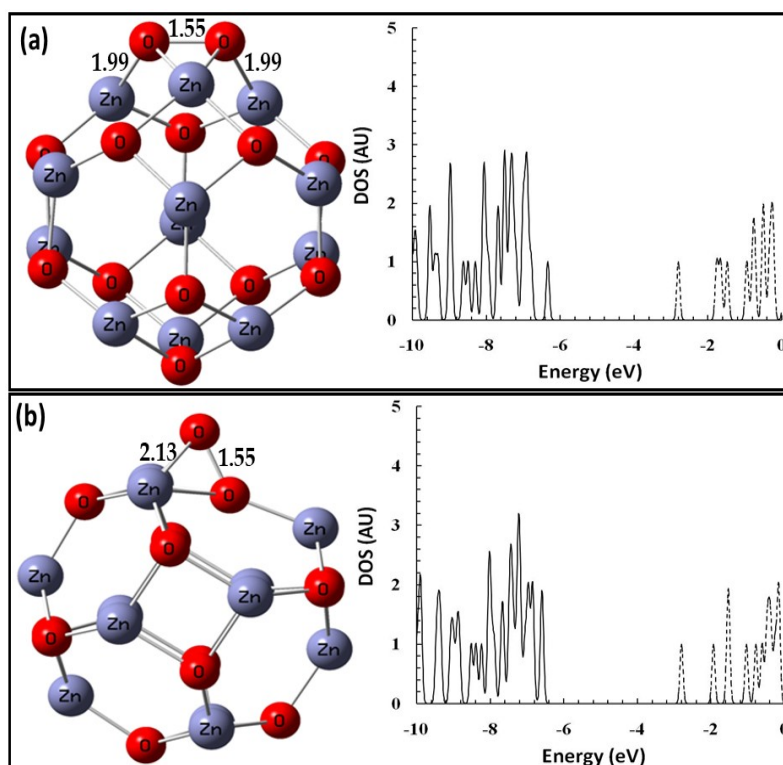


Figure 4. Optimized structures and DOSs of O atom adsorption on the Zn₁₂O₁₂ nanocage. (a) complex a, and (b) complex b. The distances are in Å, and the DOS is in arbitrary units. The solid and dashed lines represent the occupied and virtual states, respectively.

This strong interaction is attributed to the charge transfer from the Zn₁₂O₁₂ nanocage to the adsorbed O atom. As indicated by the DOS in Figure 4, the HOMO–LUMO energy gaps (E_g) of O/Zn₁₂O₁₂ for complexes (a) and (b) were reduced (to 3.53 and 3.78 eV, respectively) compared with that of the pristine Zn₁₂O₁₂ nanocage (4.02 eV; Table 1). Furthermore, for O/Zn₁₂O₁₂ complexes (a) and (b), increases of 0.24 and 0.12 eV, respectively, were observed for the Fermi level (E_{FL}), and the dipole moment increased to 2.03 and 0.72, respectively. This indicated that the deposited O atom significantly affected the electronic properties of the Zn₁₂O₁₂ nanocage, and consequently may have affected its ability to adsorb CHCl₃ molecules.

3.4. CHCl₃ Interaction with O Atoms Deposited on the Zn₁₂O₁₂ Nanocage

The CHCl₃ molecule could interact via its H head or Cl head, and the O atom could be deposited on the Zn or O sites of the nanocage; thus, there were four possible geometric structures for the CHCl₃/O/Zn₁₂O₁₂ complexes. Consequently, we performed geometric optimization for the four aforementioned CHCl₃/O/Zn₁₂O₁₂ complexes. During the optimization process, we found only three stable CHCl₃/O/Zn₁₂O₁₂ complexes, as shown in Figure 5. The properties of the interaction among the CHCl₃ molecule, deposited O atom, and Zn₁₂O₁₂ nanocage are presented in Table 4.

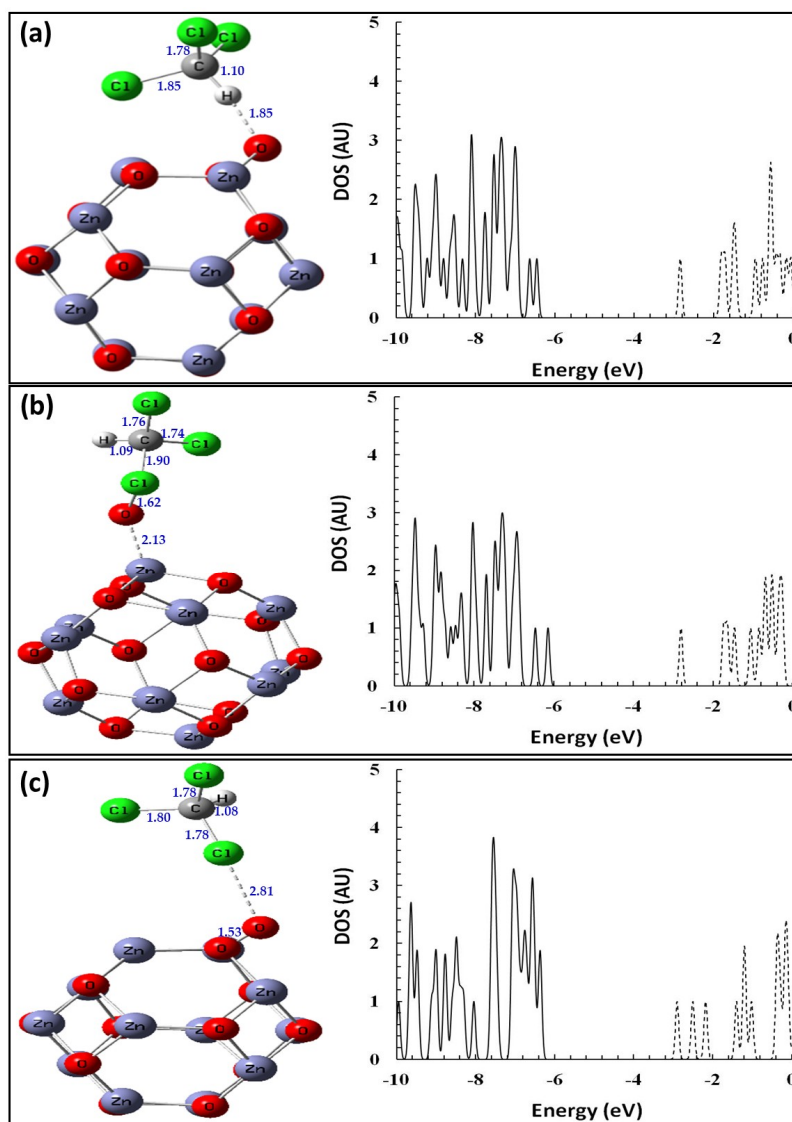


Figure 5. Optimized structures and DOSs for the $\text{CHCl}_3/\text{O}/\text{Zn}_{12}\text{O}_{12}$ nanocage. (a) complex a, (b) complex b, and (c) complex c. The distances are in Å, and the DOS is in arbitrary units. The solid and dashed lines represent the occupied and virtual states, respectively.

Table 4. Electronic properties of the isomeric configurations of the $\text{CHCl}_3/\text{O}/\text{Zn}_{12}\text{O}_{12}$ complexes, namely: adsorption energy (E_{ads} ; eV), binding energy (E_b ; eV), HOMO (eV), LUMO (eV), Fermi level (E_{FL} ; eV), HUMO–LUMO energy gap (E_g ; eV), NBO charge (Q ; au).

System	(a)	(b)	(c)
E_{ads}	−2.44	−1.98	−0.92
E_b	−0.68	−0.15	−2.46
E_{HOMO}	−6.45	−6.13	−6.30
E_{LUMO}	−2.81	−2.85	−2.98
E_{FL}	−4.63	−4.49	−4.64
E_g	3.64	3.27	3.32
Q_{CHCl_3}	0.07	0.03	0.86
Q_{O}	−0.63	−0.62	−0.76
Q_{ZnO}	0.56	0.59	−0.10
D	1.92	2.35	8.26

The adsorption energies (E_{ads}) for the complexes ranged from -0.92 to -2.44 eV. These values indicate a chemical interaction, which may have been due to a charge transfer. This can be explained by the NBO analysis, which revealed that in complexes (a) and (b), the deposited O atom gained negative charges of $-0.63|e|$ and $-0.62|e|$, respectively. These charges were mainly transferred from the $\text{Zn}_{12}\text{O}_{12}$ nanocage, which gained positive charges of $0.56|e|$ and $0.59|e|$, respectively. Additionally, there was a small charge from the CHCl_3 molecule, which gained positive charges of $0.07|e|$ and $0.03|e|$, respectively. However, in complex (c), the charge was transferred from the CHCl_3 molecule, which gained a positive charge of $0.86|e|$, to both the $\text{Zn}_{12}\text{O}_{12}$ nanocage and the deposited O atom, which gained negative charges of $-0.10|e|$ and $-0.76|e|$, respectively. Clearly, the nature of the interaction in complex (c) was significantly different from those for complexes (a) and (b). This led to different binding energies between the CHCl_3 fragment and the $\text{O}/\text{Zn}_{12}\text{O}_{12}$ fragment of the $\text{CHCl}_3/\text{O}/\text{Zn}_{12}\text{O}_{12}$ complexes, which were -0.68 , -0.15 , and -2.46 eV for complexes (a), (b), and (c), respectively. Such interactions between CHCl_3 and the $\text{O}/\text{Zn}_{12}\text{O}_{12}$ nanocage led to an increase in the Fermi level (E_{FL}), from -4.64 to -4.49 eV, as well as a reduction of the HOMO–LUMO energy gaps (E_g), from 3.27 to 3.64 eV for the $\text{CHCl}_3/\text{O}/\text{Zn}_{12}\text{O}_{12}$ complexes, compared with 4.02 eV for the pristine $\text{Zn}_{12}\text{O}_{12}$ nanocage.

To examine the effect of the CHCl_3 concentration on the interaction with the $\text{O}/\text{Zn}_{12}\text{O}_{12}$ nanocage, we performed geometric optimizations for n CHCl_3 molecules ($n = 1, 2, 3$, and 4), adsorbed simultaneously over n deposited O atoms on the $\text{Zn}_{12}\text{O}_{12}$ nanocage. Each CHCl_3 molecule interacted via its Cl head with a deposited O atom on the Zn site of the $\text{Zn}_{12}\text{O}_{12}$ nanocage. This orientation yielded the highest binding energy between the CHCl_3 molecule and $\text{O}/\text{Zn}_{12}\text{O}_{12}$. The interaction energies were calculated using Equation (3). The optimized structures of $(\text{CHCl}_3)_n/\text{O}/\text{Zn}_{12}\text{O}_{12}$ and their DOSs are shown in Figure 6.

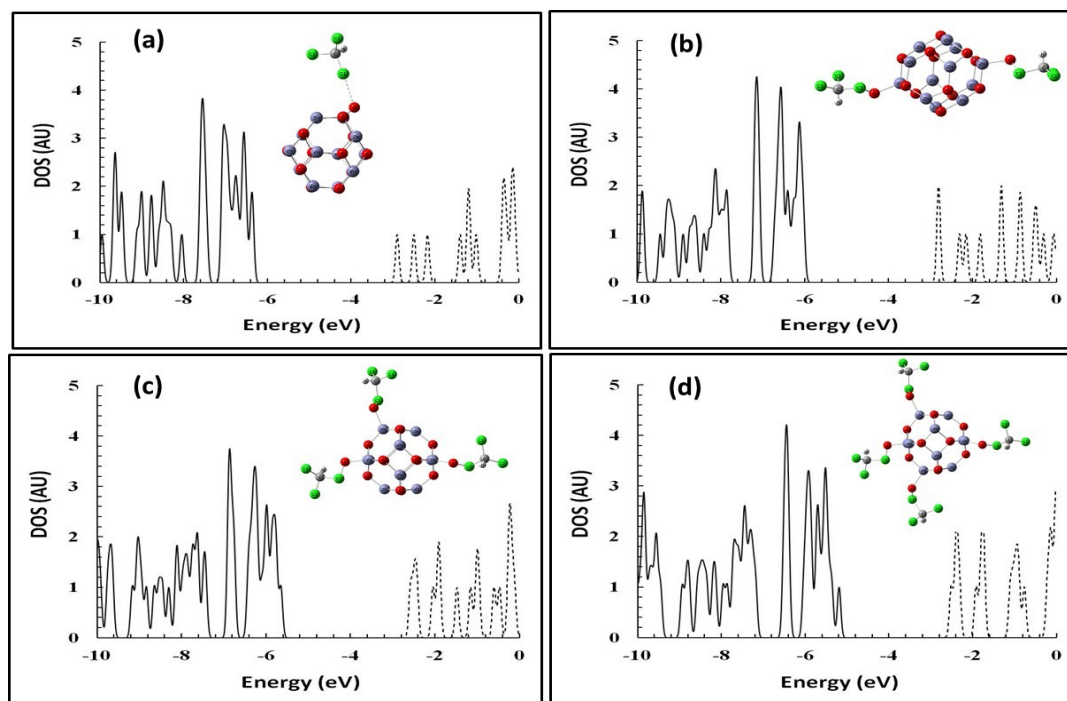


Figure 6. Optimized structures and DOSs for the $(\text{CHCl}_3)_n/\text{O}_n/\text{Zn}_{12}\text{O}_{12}$ nanocage. (a) $\text{CHCl}_3/\text{O}/\text{Zn}_{12}\text{O}_{12}$, (b) $(\text{CHCl}_3)_2/\text{O}_2/\text{Zn}_{12}\text{O}_{12}$, (c) $(\text{CHCl}_3)_3/\text{O}_3/\text{Zn}_{12}\text{O}_{12}$, and (d) $(\text{CHCl}_3)_4/\text{O}_4/\text{Zn}_{12}\text{O}_{12}$. The distances are in Å, and the DOS is in arbitrary units. The solid and dashed lines represent the occupied and virtual states, respectively.

The interaction energies are presented in Table 5. The adsorption energy remained relatively constant (approximately -0.96 eV) for the first three CHCl_3 interacting molecules, and decreased for the fourth CHCl_3 molecule (to -0.86 eV). Furthermore, as the number of adsorbed CHCl_3 molecules

increased, the average acquired positive charges on CHCl_3 (Q_{CHCl_3}) decreased, and the negativity of the average charges on the deposited O atom (Q_{O}) decreased, while the negativity of the charges on the $\text{Zn}_{12}\text{O}_{12}$ nanocage increased. Additionally, with the increasing number of adsorbed CHCl_3 molecules, the Fermi level (E_{FL}) increased and the HOMO–LUMO energy gap (E_{g}) decreased, compared with the pristine $\text{Zn}_{12}\text{O}_{12}$ nanocages. The dipole moment of $(\text{CHCl}_3)_n/\text{O}/\text{Zn}_{12}\text{O}_{12}$ was sensitive to the number of CHCl_3 molecules.

Table 5. Electronic properties of the $(\text{CHCl}_3)_n/(\text{O})_n/\text{Zn}_{12}\text{O}_{12}$ complexes, namely: adsorption energy (E_{ads} ; eV), HOMO (eV), LUMO (eV), Fermi level (E_{FL} ; eV), HOMO–LUMO energy gap (E_{g} ; eV), NBO charge (Q ; au), and dipole moment (D ; Debye).

System	(a)	(b)	(c)	(d)
	$n = 1$	$n = 2$	$n = 3$	$n = 4$
E_{ads}	−0.92	−0.96	−0.96	−0.86
E_{HOMO}	−6.30	−6.03	−5.65	−5.19
E_{LUMO}	−2.98	−2.81	−2.57	−2.51
E_{FL}	−4.64	−4.42	−4.11	−3.85
E_{g}	3.32	3.22	3.08	2.68
Q_{CHCl_3}	0.86	0.77	0.74	0.74
Q_{O}	−0.76	−0.61	−0.59	−0.58
Q_{ZnO}	−0.10	−0.33	−0.47	−0.62
D	8.26	3.26	4.15	6.45

3.5. $\text{Zn}_{12}\text{O}_{12}$ Nanocage as a Sensor for CHCl_3

It has been observed that during the adsorption process, the change in the HOMO–LUMO energy gap (E_{g}) is related to the sensitivity of the sorbent for the adsorbate. However, the reduction of E_{g} of the cluster significantly affects the electrical conductivity, as indicated by the following equation [52]:

$$\sigma \propto e^{(-E_{\text{g}}/2KT)} \quad (5)$$

where σ represents the electrical conductivity, K represents Boltzmann’s constant, and T represents the temperature. According to Equation (5) and the E_{g} values in Tables 1 and 2, the adsorption of the CHCl_3 molecule in the gas phase did not lead to significant changes in the E_{g} of the $\text{Zn}_{12}\text{O}_{12}$ nanocage. According to Tables 4 and 5, the CHCl_3 molecule adsorption over the oxygenated ZnO significantly reduced the E_{g} values.

The energy difference between the nucleophile HOMO and electrophile LUMO is one of the important factors for HOMO–LUMO interactions. As previously mentioned, the chemical bonding between CHCl_3 and the oxygenated ZnO cluster in the $\text{CHCl}_3/\text{O}/\text{Zn}_{12}\text{O}_{12}$ complexes is due to the charge-transfer mechanism. It can be explained as the contribution from the HOMO of the $\text{O}/\text{Zn}_{12}\text{O}_{12}$ cluster to the vacant LUMO of the CHCl_3 molecule. Figure 7 shows the surfaces of the frontier molecular orbitals (FMOs; HOMO/LUMO) for CHCl_3 , $\text{Zn}_{12}\text{O}_{12}$, $\text{O}/\text{Zn}_{12}\text{O}_{12}$, and $\text{CHCl}_3/\text{O}/\text{Zn}_{12}\text{O}_{12}$. The HOMO and the LUMO of the $\text{Zn}_{12}\text{O}_{12}$ cluster are localized on the Zn and O sites, respectively. Thus, the Zn sites are electrophilic centers, whereas the O sites are nucleophilic centers. This explains why the H atom of CHCl_3 is attached to the O site in the most stable structure of the $\text{CHCl}_3/\text{Zn}_{12}\text{O}_{12}$ complex. Additionally, the HOMO of the $\text{O}/\text{Zn}_{12}\text{O}_{12}$ cluster is localized around the deposited O atom. This explains why CHCl_3 is attracted to the deposited atom of the $\text{O}/\text{Zn}_{12}\text{O}_{12}$ cluster.

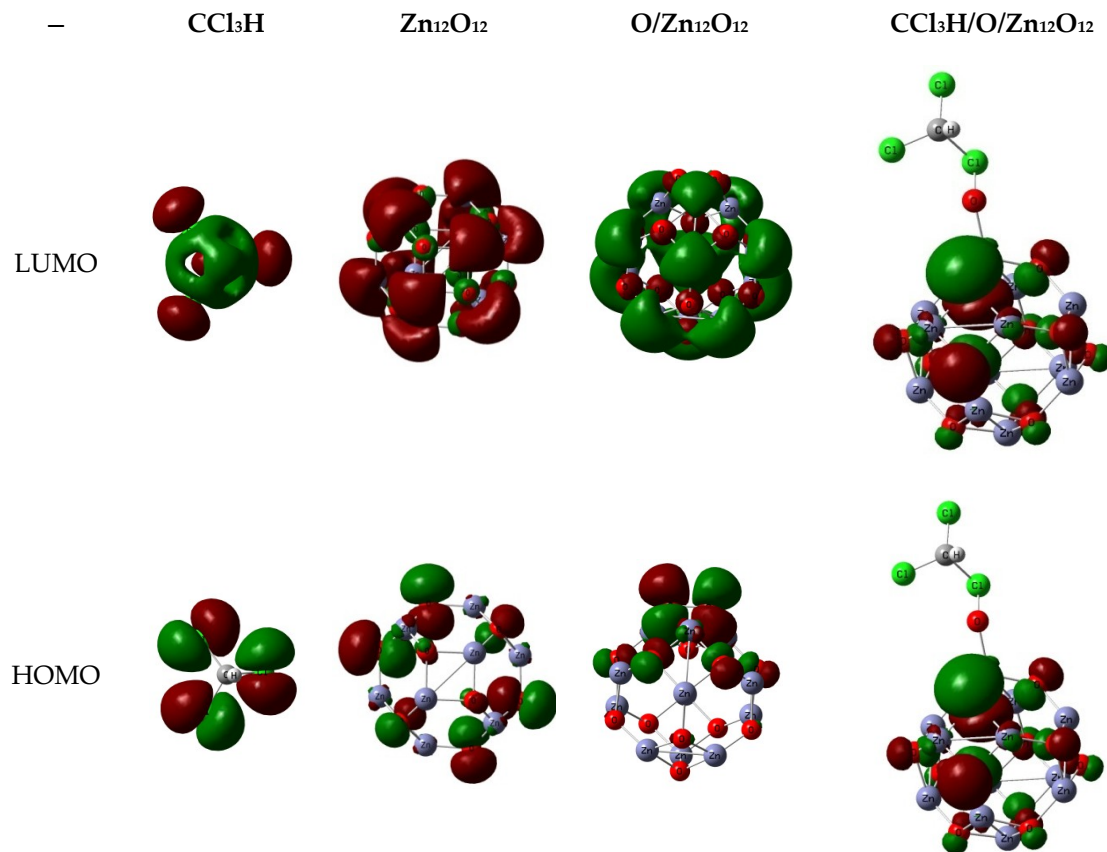


Figure 7. Frontier molecular orbital (FMO) surfaces (HOMO–LUMO) for CHCl_3 , $\text{Zn}_{12}\text{O}_{12}$, $\text{O}/\text{Zn}_{12}\text{O}_{12}$, and $\text{CHCl}_3/\text{O}/\text{Zn}_{12}\text{O}_{12}$.

Figure 8 shows the energy diagrams of the FMOs (HOMO/LUMO) for CHCl_3 , $\text{Zn}_{12}\text{O}_{12}$, $\text{O}/\text{Zn}_{12}\text{O}_{12}$, and $\text{CHCl}_3/\text{O}/\text{Zn}_{12}\text{O}_{12}$. Our FMO studies revealed that the deposited O atom increased the HOMO of the ZnO cluster from -6.81 to -6.32 eV. Consequently, the energy gap between the HOMO of ZnO and the LUMO of CHCl_3 decreased, making the charge transfer from the $\text{O}/\text{Zn}_{12}\text{O}_{12}$ cluster to the CHCl_3 easier than that from the pristine $\text{Zn}_{12}\text{O}_{12}$ cluster. Thus, the $\text{O}/\text{Zn}_{12}\text{O}_{12}$ cluster is more sensitive to the CHCl_3 molecule than the pristine $\text{Zn}_{12}\text{O}_{12}$ cluster.

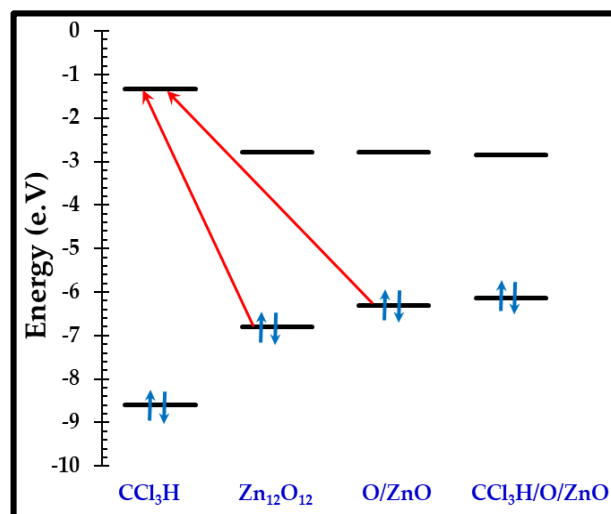


Figure 8. Energy diagram of the FMOs (HOMO/LUMO) for CHCl_3 , $\text{Zn}_{12}\text{O}_{12}$, $\text{O}/\text{Zn}_{12}\text{O}_{12}$, and $\text{CHCl}_3/\text{O}/\text{Zn}_{12}\text{O}_{12}$.

4. Conclusions

A DOS study of chloroform sensing, based on ZnO nanocrystals, was performed via calculations implemented using the Gaussian 09 suite of programs. A geometric optimization was performed for the ZnO nanocrystal. The DOS for the ZnO nanocrystal was calculated. The calculated gap between the HOMO and the LUMO was found to be 4.02 eV. Furthermore, the effect of the concentration of CHCl_3 on its adsorption over the ZnO nanocrystals was investigated. The results indicated that the electrical properties of ZnO were not affected by the concentration of CHCl_3 . Additionally, the effect of depositing O atoms on the ZnO adsorption properties was examined. The results indicated that the adsorption of CHCl_3 on the oxygenated ZnO reduced its bandgap. The findings of this study confirm that the deposition of O on a ZnO nanocluster increases its sensitivity to CHCl_3 , and may facilitate CHCl_3 removal or detection.

Author Contributions: Conception and design of the experiments, H.Y.A., H.M.B. and A.U.; implementation of the experiments, H.Y.A., H.M.B. and A.U.; analysis of the data, contribution of the analysis tools, and writing and revision of the paper, H.Y.A., H.M.B., A.U., H.F. and O.Y.A.

Funding: This work is funded by Deanship of Scientific Research at King Saud University under the research groups grant (No. RG-1435-052).

Acknowledgments: The authors would like to extend their sincere appreciation to the Deanship of Scientific Research at King Saud University for funding this research group (No. RG-1435-052). The authors thank RSSU at King Saud University for their technical support.

Conflicts of Interest: The authors declare no conflict of interest.

References

1. Batzill, M.; Diebold, U. The surface and materials science of tin oxide. *Prog. Surf. Sci.* **2005**, *79*, 47–154. [[CrossRef](#)]
2. Wang, Z.-H.; Yang, C.-C.; Yu, H.-C.; Peng, Y.-M.; Su, Y.-K. Electron emission enhanced properties of gold nanoparticle-decorated ZnO nanosheets grown at room temperature. *Sci. Adv. Mater.* **2018**, *10*, 1675–1679. [[CrossRef](#)]
3. Kim, E.-B.; Lee, J.-E.; Akhtar, M.S.; Ameen, S.; Fijahi, L.; Seo, H.-K.; Shin, H.-S. Electrical sensor based on hollow ZnO spheres for hydrazine detection. *J. Nanoelectron. Optoelectron.* **2018**, *13*, 1769–1776. [[CrossRef](#)]
4. Bader, C. The dangers of chloroform, etc., and the nitrite of amyl. *Lancet* **1875**, *105*, 644. [[CrossRef](#)]
5. Featherstone, P.J.; Ravindran, H. Townley's chloroform inhaler. *J. Anesth. Hist.* **2018**, *4*, 103–108. [[CrossRef](#)] [[PubMed](#)]
6. Verma, P.; Tordik, P.; Nosrat, A. Hazards of improper dispensary: Literature review and report of an accidental chloroform injection. *J. Endod.* **2018**, *44*, 1042–1047. [[CrossRef](#)]
7. Selby, R. Chloroform-Its benefits and its dangers. *Lancet* **1848**, *51*, 190. [[CrossRef](#)]
8. Zhang, K.; Zhang, H.; Liu, R.; Yang, Z.; Yuan, Y.; Wang, F. Fabrication of aluminum doped zinc oxide thin films with various microstructures for gas sensing application. *Sci. Adv. Mater.* **2018**, *10*, 367–372. [[CrossRef](#)]
9. Ahad, I.Z.M.; Harun, S.W.; Gan, S.N.; Phang, S.W. Polyaniline (PAni) optical sensor in chloroform detection. *Sens. Actuators B Chem.* **2018**, *261*, 97–105. [[CrossRef](#)]
10. Sheng, K.; Lu, H.; Sun, A.; Wang, Y.; Liu, Y.; Chen, F.; Bian, W.; Li, Y.; Kuang, R.; Sun, D. A naked-eye colorimetric sensor for chloroform. *Chin. Chem. Lett.* **2019**, *30*, 895–898. [[CrossRef](#)]
11. Sharma, S.; Nirkhe, C.; Pethkar, S.; Athawale, A.A. Chloroform vapour sensor based on copper/polyaniline nanocomposite. *Sens. Actuators B Chem.* **2002**, *85*, 131–136. [[CrossRef](#)]
12. Wang, K.; Li, S.; Jiang, Y.; Hu, M.; Zhai, Q.G. A pillar-layered metal-organic framework as luminescent sensor for selective and reversible response of chloroform. *J. Solid State Chem.* **2017**, *247*, 39–42. [[CrossRef](#)]
13. Zhang, K.; Zhang, H.; Sun, S.; Yang, Z.; Yuan, Y.; Wang, F. Enhanced gas sensing properties based on ZnO-decorated nickel oxide thin films for formaldehyde detection. *Sci. Adv. Mater.* **2018**, *10*, 373–378. [[CrossRef](#)]
14. Kumar, R.; Al-Dossary, O.; Kumar, G.; Umar, A. Zinc oxide nanostructures for NO_2 gas sensor applications: A review. *Nano Micro Lett.* **2015**, *7*, 97–120. [[CrossRef](#)] [[PubMed](#)]

15. Jia, R.; Xie, P.; Feng, Y.; Chen, Z.; Umar, A.; Wang, Y. Dipole-modified graphene with ultrahigh gas sensibility. *Appl. Surf. Sci.* **2018**, *440*, 409–414. [[CrossRef](#)]
16. Zhou, Q.; Xu, L.; Umar, A.; Chen, W.; Kumar, R. Pt nanoparticles decorated SnO₂ nanoneedles for efficient CO gas sensing applications. *Sens. Actuators B Chem.* **2018**, *256*, 656–664. [[CrossRef](#)]
17. Umar, A.; Alshahrani, A.A.; Algarni, H.; Kumar, R. CuO nanosheets as potential scaffolds for gas sensing applications. *Sens. Actuators B Chem.* **2017**, *250*, 24–31. [[CrossRef](#)]
18. Al-Hadeethi, Y.; Umar, A.; Ibrahim, A.A.; Al-Heniti, S.H.; Kumar, R.; Baskoutas, S.; Raffah, B.M. Synthesis, characterization and acetone gas sensing applications of Ag-doped ZnO nanoneedles. *Ceram. Int.* **2017**, *43*, 6765–6770. [[CrossRef](#)]
19. Umar, A.; Lee, J.-H.; Kumar, R.; Al-Dossary, O. Synthesis and characterization of CuO nanodisks for high-sensitive and selective ethanol gas sensor applications. *J. Nanosci. Nanotechnol.* **2017**, *17*, 1455–1459. [[CrossRef](#)]
20. Al-Hadeethi, Y.; Umar, A.; Al-Heniti, S.H.; Kumar, R.; Kim, S.H.; Zhang, X.; Raffah, B.M. 2D Sn-doped ZnO ultrathin nanosheet networks for enhanced acetone gas sensing application. *Ceram. Int.* **2017**, *43*, 2418–2423. [[CrossRef](#)]
21. Nam, G.; Leem, J.Y. A new technique for growing ZnO nanorods over large surface areas using graphene oxide and their application in ultraviolet sensors. *Sci. Adv. Mater.* **2018**, *10*, 405–409. [[CrossRef](#)]
22. Zhang, N.; Yu, K.; Li, Q.; Zhu, Z.Q.; Wan, Q.J. Room-temperature high-sensitivity H₂S gas sensor based on dendritic ZnO nanostructures with macroscale in appearance. *Appl. Phys.* **2008**, *103*, 104305. [[CrossRef](#)]
23. Jimenez, I.; Arbiol, J.; Dezaneeau, G.; Cornet, A.; Morante, J.R. Crystalline structure, defects and gas sensor response to NO₂ and H₂S of tungsten trioxide nanopowders. *Sens. Actuators B Chem.* **2003**, *93*, 475–485. [[CrossRef](#)]
24. Chen, Z.; Wang, J.; Umar, A.; Wang, Y.; Li, H.; Zhou, G. Three-dimensional crumpled graphene-based nanosheets with ultrahigh NO₂ gas sensibility. *ACS Appl. Mater. Interfaces* **2017**, *9*, 11819–11827. [[CrossRef](#)]
25. Umar, A.; Akhtar, M.S.; Al-Assiri, M.S.; Al-Salami, A.E.; Kim, S.H. Composite CdO-ZnO hexagonal nanocones: Efficient materials for photovoltaic and sensing applications. *Ceram. Int.* **2018**, *44*, 5017–5024. [[CrossRef](#)]
26. Umar, A. *Encyclopedia of Semiconductor Nanotechnology*; American Scientific Publishers: Los Angeles, CA, USA, 2017.
27. Choi, H.J.; Lee, Y.M.; Boo, J.H. Well-aligned ZnO nanorods assisted with close-packed polystyrene monolayer for quartz crystal microbalance. *Sci. Adv. Mater.* **2018**, *10*, 610–615. [[CrossRef](#)]
28. Yang, J.; Yi, W.; Zhang, L.; Li, T.; Chao, Z.; Fan, J. Facile fabrication of ZnO nanomaterials and their photocatalytic activity study. *Sci. Adv. Mater.* **2018**, *10*, 1721–1728. [[CrossRef](#)]
29. Umar, A.; Hahn, Y.B. *Metal Oxide Nanostructures and Their Applications*; American Scientific Publishers: Los Angeles, CA, USA, 2010.
30. Wang, J.X.; Sun, X.W.; Yang, Y.; Huang, H.; Lee, Y.C.; Tan, O.K.; Vayssieres, L. Hydrothermally grown oriented ZnO nanorod arrays for gas sensing applications. *Nanotechnology* **2006**, *17*, 4995–4998. [[CrossRef](#)]
31. Paraguay, F.; Miki-Yoshida, M.; Morales, J.; Solis, J.; Estrada, L.W. Influence of Al, In, Cu, Fe and Sn dopants on the response of thin film ZnO gas sensor to ethanol vapour. *Thin Solid Films* **2000**, *373*, 137–140. [[CrossRef](#)]
32. Chaudhary, S.; Kaur, Y.; Umar, A.; Chaudhary, G.R. Ionic liquid and surfactant functionalized ZnO nanoadsorbent for recyclable proficient adsorption of toxic dyes from waste water. *J. Mol. Liq.* **2016**, *224*, 1294–1304. [[CrossRef](#)]
33. Guo, R.; Cheng, X.; Gao, S.; Zhang, X.; Xu, Y.; Zhao, H.; Huo, L. Highly selective detection of saturated vapors of abused drugs by ZnO nanorod bundles gas sensor. *Appl. Surf. Sci.* **2019**, *485*, 266–273. [[CrossRef](#)]
34. Shao, C.; Chang, Y.; Long, Y. High performance of nanostructured ZnO film gas sensor at room temperature. *Sens. Actuators B Chem.* **2014**, *204*, 666–672. [[CrossRef](#)]
35. Ghenaatian, H.R.; Baei, M.T.; Hashemian, S. Zn₁₂O₁₂ nano-cage as a promising adsorbent for CS₂ capture. *Superlattices Microstruct.* **2013**, *58*, 198–204. [[CrossRef](#)]
36. Baei, M.T.; Tabar, M.B.; Hashemian, S. Zn₁₂O₁₂ fullerene-like cage as a potential sensor for SO₂ detection. *Adsorpt. Sci. Technol.* **2013**, *3*, 469–476. [[CrossRef](#)]
37. Ammar, H.Y. CH₂O adsorption on M (M = Li, Mg and Al) atom deposited ZnO nano-cage: DFT study. *Key Eng. Mater.* **2018**, *786*, 384. [[CrossRef](#)]

38. Mayya, D.S.; Prasad, P.; Kumar, J.R.N.; Aswanth, P.; Mayur, G.; Aakanksha, M.; Bindushree, N. Nanocrystalline zinc oxide thin film gas sensor for detection of hydrochloric acid, ethanolamine, and chloroform. *Int. J. Adv. Res. Sci. Eng. Technol.* **2018**, *7*, 809–818.
39. Frisch, M.J.; Trucks, G.W.; Schlegel, H.B.; Scuseria, G.E.; Robb, M.A.; Cheeseman, J.R.; Montgomery, J.A., Jr.; Vreven, T.; Kudin, K.N.; Burant, J.C.; et al. *Gaussian 09*; Gaussian, Inc.: Wallingford, CT, USA, 2004.
40. Becke, A.D. Density-functional thermochemistry. III. The role of exact exchange. *J. Chem. Phys.* **1993**, *98*, 5648. [[CrossRef](#)]
41. Vosko, S.H.; Wilk, L.; Nusair, M. Accurate spin-dependent electron liquid correlation energies for local spin density calculations: A critical analysis. *Can. J. Phys.* **1980**, *58*, 1200–1211. [[CrossRef](#)]
42. Becke, A.D. Density-functional exchange-energy approximation with correct asymptotic behavior. *Phys. Rev. A* **1988**, *38*, 3098. [[CrossRef](#)]
43. Lee, C.; Yang, W.; Parr, R.G. Development of the Colle-Salvetti correlation-energy formula into a functional of the electron density. *Phys. Rev. B* **1988**, *37*, 785. [[CrossRef](#)]
44. Miehlich, B.; Savin, A.; Stoll, H.; Preuss, H. Results obtained with the correlation energy density functionals of Becke and Lee, Yang and Parr. *Chem. Phys. Lett.* **1989**, *157*, 200–206. [[CrossRef](#)]
45. Beheshtian, J.; Peyghan, A.A.; Bagheri, Z. Adsorption and dissociation of Cl₂ molecule on ZnO nanocluster. *Appl. Surf. Sci.* **2012**, *258*, 8171. [[CrossRef](#)]
46. Boyle, N.M.O.; Tenderholt, A.L.; Langner, K.M. Cclib: A library for package-independent computational chemistry algorithms. *J. Comp. Chem.* **2008**, *29*, 839. [[CrossRef](#)] [[PubMed](#)]
47. Glendening, E.D.; Reed, A.E.; Carpenter, J.E.; Weinhold, F. *NBO Program, Version 3.1*; University of Wisconsin: Madison, WI, USA, 2001.
48. Narayanaswamy, A.; Xu, H.F.; Pradhan, N.; Peng, X.G. Crystalline nanoflowers with different chemical compositions and physical properties grown by limited ligand protection. *Angew. Chem. Int. Ed.* **2006**, *45*, 5361. [[CrossRef](#)] [[PubMed](#)]
49. Joshi, P.; Shewale, V.; Pandey, R.; Shanker, V.; Hussain, S.; Karna, S.P. Site specific interaction between ZnO nanoparticles and tryptophan: A first principles quantum mechanical study. *Phys. Chem. Chem. Phys.* **2011**, *13*, 476. [[CrossRef](#)] [[PubMed](#)]
50. Shalabi, A.S.; Abdel Aal, S.; Kamel, M.A.; Taha, H.O.; Ammar, H.Y.; Abdel Halim, W.S. The role of oxidation states in F_{A1} Tlⁿ⁺ (n = 1, 3) lasers and CO interactions at the (1 0 0) surface of NaCl: An ab initio study. *Chem. Phys.* **2006**, *328*, 8–16. [[CrossRef](#)]
51. Shalabi, A.S.; Abdel Aal, S.; Ammar, H.Y. Artificial polarization effects on F_{A1}:Sr²⁺ lasers and NO interactions at NaCl (001) surface: First principles calculations. *J. Mol. Struct. Theochem.* **2007**, *823*, 47–58. [[CrossRef](#)]
52. Li, S. *Semiconductor Physical Electronics*, 2nd ed.; Springer: New York, NY, USA, 2006.

